



# Fabrication of morphology-controlled TiO<sub>2</sub> photocatalyst nanoparticles and improvement of photocatalytic activities by modification of Fe compounds

著者	Ohno Teruhisa, Lee Szu Ying, Yang Yin
journal or publication title	Rare metals
volume	34
number	5
page range	291-300
year	2015-05
URL	<a href="http://hdl.handle.net/10228/00006501">http://hdl.handle.net/10228/00006501</a>

doi: [info:doi/10.1007/s12598-015-0483-8](https://doi.org/10.1007/s12598-015-0483-8)

# **Fabrication of morphology-controlled TiO<sub>2</sub> photocatalyst nanoparticles and improvement of photocatalytic activities by modification of Fe compounds**

Teruhisa Ohno, Yin Yang

Department of Materials Science, Graduate School of Engineering, Kyushu Institute of Technology, Fukuoka 804-8550, Japan  
tohno@che.kyutech.ac.jp

## **Abstract**

Our previous studies suggested that redox reaction proceeded separately on specific exposed crystal faces of TiO<sub>2</sub> nanoparticles. Site-selective deposition of metal or metal oxide on TiO<sub>2</sub> specific exposed crystal faces successfully proceeded using the unique reactivity properties on the surface of TiO<sub>2</sub> nanoparticles under photoexcitation.

A remarkable improvement of photocatalytic activity of shape-controlled brookite and rutile TiO<sub>2</sub> nanorods with modification of Fe<sup>3+</sup> compounds was observed under visible light. Crystal face-selective metal compound modification on exposed crystal faces of TiO<sub>2</sub> nanorods with brookite and rutile phases were successfully prepared. Brookite and rutile TiO<sub>2</sub> nanorods prepared by site-selective modification with metal compounds should be ideal visible-light responsive TiO<sub>2</sub> photocatalysts because of the remarkable suppression of back electron transfer from TiO<sub>2</sub> to oxidized metal compounds on the surface of the TiO<sub>2</sub> nanorod with a brookite or rutile phase.

In this manuscript, the development of exposed crystal face-controlled TiO<sub>2</sub> nanorods with rutile and brookite phases was described. The obtained rutile and brookite TiO<sub>2</sub> nanorod, showing remarkably high activity for degradation of organic compounds compared to the photocatalytic activities of anatase fine particles (ST-01), is one of the most active commercially available photocatalysts for environmental cleanup in Japan. The technology of visible light-responsive treatment for morphology-controlled rutile and brookite TiO<sub>2</sub> nanorods by crystal face-selective modification of Fe<sup>3+</sup> compounds was also discussed in this paper. The Fe<sup>3+</sup> compound-modified rutile and brookite TiO<sub>2</sub> nanorods show much higher activity than that of conventional visible light-responsive N-doped TiO<sub>2</sub>, which is commercially available in Japan.

**Keywords** Morphology-controlled TiO<sub>2</sub>; Separation of reaction sites; Visible-light responsive TiO<sub>2</sub> loaded with Fe<sup>3+</sup>

## 1. Introduction

TiO<sub>2</sub> has been intensively investigated over the past several decades for its environmental cleanup and solar light energy conversion applications because of its stable physical-chemical properties, low cost and high activity [1-9]. TiO<sub>2</sub> has three kinds of crystal faces: rutile, anatase and brookite. The particle shapes, nano-scale morphologies, and crystallinity of rutile were clarified and can be controlled [9-11]. The surface chemistry of single crystalline rutile particles is also studied intensively because their chemical activity depends greatly on surface structures and exposed crystal faces [12].

Well-crystallized faceted TiO<sub>2</sub> nanoparticles showed a drastic improvement of photocatalytic activity compared to that of normal spherical TiO<sub>2</sub> fine particles with poor crystallinity [13]. Therefore, attention has been paid to the preparation of TiO<sub>2</sub> nanoparticles with control of exposed crystal faces for improvement of their photocatalytic activity. Among the various methods for synthesis of TiO<sub>2</sub> nanoparticles, hydrothermal treatment is thought to be one of the best candidates for TiO<sub>2</sub> synthesis because TiO<sub>2</sub> nanoparticles with good morphology control using additives for exposing crystal faces are obtained under mild conditions. Recently, morphology-controlled TiO<sub>2</sub> nanoparticles with anatase, rutile, and brookite phases have been prepared by these techniques. [14-19]

The development of visible light-responsive TiO<sub>2</sub> photocatalysts using impurity doping has proceeded over the past few decades [20-25]. However, impurity doping sometimes increase defects in the lattice of TiO<sub>2</sub>, resulting in a decrease in photocatalytic activity because the defects work as recombination centers [26, 27]. Recently, unique visible-light responsive TiO<sub>2</sub> photocatalysts loaded with metal ions such as Fe<sup>3+</sup> and Cu<sup>2+</sup> have been reported [28-32]. This is an interesting method for fabrication of visible light-responsive TiO<sub>2</sub> without defects. However, back electron transfer between injected electrons from a metal sensitizer in the TiO<sub>2</sub> bulk and oxidized metal ions loaded on the surface of TiO<sub>2</sub> may easily proceed and result in a significant decrease in photocatalytic activity under visible light. Therefore, it is necessary for new discovery for development metal compounds modified TiO<sub>2</sub> showing visible light responsibility.

## 2. Exposed crystal face-controlled rutile TiO<sub>2</sub> nanorod

The procedure for synthesis of an exposed crystal face-controlled rutile TiO<sub>2</sub> nanorod is as follows. A chemical solution was put in a sealed Teflon-lined autoclave reactor containing an aqueous solution of titanium trichloride (TiCl<sub>3</sub>) and sodium chloride (NaCl). The solution was then put into a 200 °C oven for 48 h. The precipitate was collected and dried in a vacuum oven. Samples are

referred to as SH1 (NaCl 1 mol·L<sup>-1</sup>), SH3 (NaCl 3 mol·L<sup>-1</sup>), and SH5 (NaCl 5 mol·L<sup>-1</sup>). SH5 is the optimized preparation condition for the highest photocatalytic activity.

Reduction and oxidation sites on the exposed crystal faces of a rutile TiO<sub>2</sub> nanorod were assigned by the photodeposition technique for Pt and PbO<sub>2</sub>, respectively. A rutile TiO<sub>2</sub> nanorod aqueous suspension containing 2-propanol and hexachloroplatinic acid (H<sub>2</sub>PtCl<sub>6</sub>·6H<sub>2</sub>O) was irradiated with a mercury ultraviolet-visible (UV) lamp (light intensity: 1.0 mW·cm<sup>-2</sup>). N<sub>2</sub> gas was purged through the suspension in order to remove oxygen prior to UV irradiation. After irradiation, the color of the powder changed from white to gray-silver, and the suspension was collected (Pt-loaded rutile TiO<sub>2</sub> nanorod) and dried at 70 °C under reduced pressure for 24 h. In order to determine the oxidation site on the surface of a rutile TiO<sub>2</sub> nanorod, photodeposition of PbO<sub>2</sub> was performed by using the same light source as that in the case of photodeposition of Pt. Pt-loaded rutile TiO<sub>2</sub> nanorod suspension containing Pb(NO<sub>3</sub>)<sub>2</sub> was irradiated under an aerated condition [14-19, 33]. After the reaction, the color of the powder changed from gray-silver to brown, indicating that PbO<sub>2</sub> was deposited on the surface of the rutile TiO<sub>2</sub> nanorod. Pt and PbO<sub>2</sub> particles deposited on a rutile TiO<sub>2</sub> nanorod were analyzed by scanning electron microscope (SEM), energy dispersive X-ray spectrometry (EDX) and transmission electron microscope (TEM).

The photocatalytic activity of TiO<sub>2</sub> nanoparticles was evaluated by photodecomposition of acetaldehyde. Changes in the concentration of acetaldehyde and evolved CO<sub>2</sub> as a function of irradiation time were analyzed. TiO<sub>2</sub> powder was spread on the bottom of a glass dish, and the glass dish was placed in a Tedlar bag. 500×10<sup>-6</sup> acetaldehyde was prepared in the vessel. Irradiation was conducted at room temperature after equilibrium between the gas and adsorbed acetaldehyde was reached. A 500 W Xe-lamp with a UV-35 filter to cut off wavelengths shorter than 350 nm was used as a light source. After starting the irradiation, the decreases in acetaldehyde concentration and evolved CO<sub>2</sub> concentration were determined by using a gas chromatograph. ST-01 having anatase phase fine TiO<sub>2</sub> produced by Ishihara Sangyo CO. Ltd. and MT-600 having rutile phase produced by Teyca Co. Ltd. were usually used as reference catalysts.

XRD patterns of all of the obtained particles were assigned to pure rutile phase and no other phases were detected (Fig.1). The mean grain size was determined from Scherrer's equation. The average crystallite sizes (relative surface areas) of the samples were found to be 66.0 nm (32.8 m<sup>2</sup>·g<sup>-1</sup>), 72.7 nm (26.0 m<sup>2</sup>·g<sup>-1</sup>) and 97.2 nm (12.1 m<sup>2</sup>·g<sup>-1</sup>) for SH1, SH3 and SH5, respectively. Figure 2 shows TEM image and selected area electron diffraction (SAED) patterns. The particle morphology was rod shape as shown in TEM image. The SAED patterns of the exposed surface of the end of the rod and side surface of the rod were assigned to (111) and (110), respectively.

Figure 3 shows the photocatalytic evolution of CO<sub>2</sub> by decomposition of acetaldehyde on reference TiO<sub>2</sub> and SH5 under UV light irradiation at a light intensity of 10 mW·cm<sup>-2</sup>. Photocatalytic activities of rutile TiO<sub>2</sub> nanorods were much higher than those of MT-600 and ST-01. The order of photocatalytic activities was SH5 > ST-01 > MT-600B as shown in Fig.3. Separation of reaction sites on the surface of a rutile TiO<sub>2</sub> nanorod might be important for improvement of its photocatalytic activity. Moreover, it is expected that the efficiency of electron-hole separation would be enhanced because of the difference in the number of trap sites for electrons such as Ti ions and for holes such as oxygen on the exposed crystal surfaces.

Figure 4 shows SEM image of rutile TiO<sub>2</sub> nanorods loaded with Pt for the reduction site ((110) face) and loaded with PbO<sub>2</sub> for the oxidation site ((111) face). Spatial separation of reaction sites on exposed crystal face-controlled rutile TiO<sub>2</sub> nanorods is thought to be effective for improvement of photocatalytic reactions because of the suppression of back reaction on the surface of the TiO<sub>2</sub> photocatalyst.

Different surface energy levels of the conduction and valence bands are expected for different crystal faces of TiO<sub>2</sub> because of the characteristic of atomic arrangements of these faces. For instance, trapped holes are mainly accumulated at an oxygen-rich crystal face, which might be assigned to an oxidation site. On the other hand, crystal face rich in Ti<sup>4+</sup> atoms results in the accumulation of electrons to generate Ti<sup>3+</sup>, which might be assigned to a reduction site. These properties lead to the separation of electrons and holes [14]. The effective separation of oxidation and reduction sites of rutile TiO<sub>2</sub> nanorods suggests that the electronic energy levels of the (110) face are lower than those of the (111) face as shown in Fig.4 [34]. The large specific surface areas and small crystal sizes as well as high crystallinity of TiO<sub>2</sub> might play important roles in the enhancement of photocatalytic activities. In addition, spatial separation of reaction sites on the photocatalyst nanoparticle by controlling the exposed crystal surface of a rutile TiO<sub>2</sub> nanorod is a more important factor for improvement of photocatalytic activity because a rutile TiO<sub>2</sub> nanorod with a small surface area (10-30 m<sup>2</sup>·g<sup>-1</sup>) showed a higher photocatalytic activity than that of ST-01 with a large surface area (300 m<sup>2</sup>·g<sup>-1</sup>).

### 3. Visible light-responsive rutile TiO<sub>2</sub> nanorod modified with Fe<sup>3+</sup> compounds

The procedure for non-site-selective modification of Fe<sup>3+</sup> compounds on the entire surface of rutile TiO<sub>2</sub> nanorods is as follows. An aqueous suspension of morphology-controlled rutile TiO<sub>2</sub> nanorods with an aqueous solution of Fe(NO<sub>3</sub>)<sub>3</sub> was stirred under an aerated condition. After filtration, the residue was washed with deionized water and dried under reduced pressure.

The procedure for preparation of visible-light responsive rutile TiO<sub>2</sub> nanorods site-selective modified with Fe<sup>3+</sup> compounds is as follows. An aqueous suspension consisting of rutile TiO<sub>2</sub> nanorods and an aqueous solution of Fe(NO<sub>3</sub>)<sub>3</sub> with ethanol was stirred under an aerated condition by bubbling N<sub>2</sub> gas. Photo-reduction of Fe<sup>3+</sup> loaded on reduction crystal faces ({110} faces) of rutile TiO<sub>2</sub> nanorods proceeded during UV irradiation. Fe<sup>2+</sup> compounds on the reduction sites of rutile TiO<sub>2</sub> nanorods, which were generated by reduction of Fe<sup>3+</sup>, were dissolved in aqueous phase. The residue was separated by filtration immediately after the photoirradiation. The residue was washed with deionized water and dried under reduced pressure (Fig.5).

Photocatalytic activities of the samples were evaluated by photocatalytic decomposition of acetaldehyde. A glass dish containing a sample was placed in a 125 ml Tedlar bag. 500×10<sup>-6</sup> gaseous acetaldehyde was injected into the Tedlar bag, and photoirradiation was performed at room temperature. The gaseous composition in the Tedlar bag was 79% N<sub>2</sub>, 21% O<sub>2</sub>, < 0.1×10<sup>-6</sup> CO<sub>2</sub> and 500×10<sup>-6</sup> acetaldehyde, and relative humidity was 30% (ca.). An light-emitting diode (LED) emitting light at a wavelength of ca. 455 nm (±15 nm) with an intensity of 1.0 mW·cm<sup>-2</sup> was used for visible light irradiation. The concentrations of CH<sub>3</sub>CHO and CO<sub>2</sub> were estimated by gas chromatography.

Double-beam photoacoustic spectroscopy was used to elucidate the electron transfer between rutile TiO<sub>2</sub> nanorods and Fe<sup>3+</sup> compounds loaded on the oxidation sites of rutile TiO<sub>2</sub> nanorods. A TiO<sub>2</sub> sample was placed in a photoacoustic (PA) cell. The atmosphere was controlled by a flow of nitrogen containing ethanol vapor (N<sub>2</sub>+EtOH) or artificial air containing ethanol vapor (air+EtOH). An LED emitting light at ca. 625 nm was used as a probe light, and the output intensity was modulated by a digital function generator. A blue LED (emitting light at ca. 470 nm, 8.1 mW·cm<sup>-2</sup>) was also used as simultaneous continuous irradiation for photoexcitation. The PA signal acquired by a condenser microphone buried in the cell was amplified and monitored by a digital lock-in amplifier. Detailed setups of double-beam photoacoustic (DB-PA) spectroscopic measurements were reported previously [35].

The rutile TiO<sub>2</sub> nanorods were prepared according to our previous studies [15, 16]. Rutile TiO<sub>2</sub> nanorods used in this study have {110} and {111} exposed crystal faces. The specific surface area of the bare rutile rod was 12.1 m<sup>2</sup>·g<sup>-1</sup>.

The valence state of iron compounds on rutile TiO<sub>2</sub> nanorods was confirmed by XPS analysis to be trivalent state. It was reported that Fe<sup>2+</sup> was hardly adsorbed on the TiO<sub>2</sub> surface compared to Fe<sup>3+</sup> compounds [36]. Therefore, Fe<sup>2+</sup> produced by reduction of Fe<sup>3+</sup> by photoexcited electrons on reduction sites of rutile TiO<sub>2</sub> nanorods from the TiO<sub>2</sub> surface diffused into aqueous media. Our previous study suggested that reduction and oxidation on a rutile TiO<sub>2</sub> nanorod proceeded

predominantly on {110} and {111} exposed crystal faces [28]. Therefore,  $\text{Fe}^{3+}$  are expected to be mainly adsorbed on {111} faces under UV irradiation because  $\text{Fe}^{3+}$  on {110} faces are desorbed due to reduction of  $\text{Fe}^{3+}$  to  $\text{Fe}^{2+}$  (Fig.5). Modification of  $\text{Fe}^{3+}$  induced a color change from white to pale yellow as reported previously [32]. Figure 6 show UV-Vis spectra of bare and site-selective  $\text{Fe}^{3+}$ -modified rutile  $\text{TiO}_2$  nanorods and non-site-selective  $\text{Fe}^{3+}$ -modified rutile  $\text{TiO}_2$  nanorods. In the wavelength region between 400 and 500 nm of DR spectra, a red shift of the photoabsorption edge was observed.

Photocatalytic activity for decomposition of acetaldehyde over  $\text{Fe}^{3+}$ -modified rutile  $\text{TiO}_2$  nanorod was evaluated under visible light irradiation. Figure 7 shows the amount of evolved  $\text{CO}_2$  as a result of acetaldehyde degradation under visible-light irradiation for 24 h. Photocatalytic activity of  $\text{Fe}^{3+}$ -modified rutile  $\text{TiO}_2$  nanorod was higher than that of visible light-responsive N-doped  $\text{TiO}_2$  (N- $\text{TiO}_2$ ; Sumitomo Chemical Co.). This result indicates that  $\text{Fe}^{3+}$  compound modification of a rutile  $\text{TiO}_2$  nanorod induces a photocatalytic reaction under visible-light irradiation as follows [32]. The photoexcited  $\text{Fe}^{3+}$  compound loaded on a rutile  $\text{TiO}_2$  nanorod injected electrons into the conduction band of the rutile  $\text{TiO}_2$  nanorod, resulting in an oxidized state of  $\text{Fe}^{3+}$  ( $\text{Fe}^{4+}$ ). The injected electrons migrated to the surface of the rutile  $\text{TiO}_2$  nanorod and reduced oxygen species. The oxidized state of the  $\text{Fe}^{3+}$  compound ( $\text{Fe}^{4+}$ ) oxidized organic compounds such as acetaldehyde and returned to the initial state of the metal ion compound ( $\text{Fe}^{3+}$ ). A site-selective modified  $\text{Fe}^{3+}$  rutile  $\text{TiO}_2$  nanorod showed higher photocatalytic activity than that of N-doped  $\text{TiO}_2$ . Moreover, the photocatalytic activity of  $\text{Fe}^{3+}$ -modified rutile  $\text{TiO}_2$  showed a dependence on its preparation method (site-selective modified  $\text{Fe}^{3+}$  rutile  $\text{TiO}_2$  nanorod > non-site-selective modified  $\text{Fe}^{3+}$  rutile  $\text{TiO}_2$  nanorod). A plausible reason for the difference in photocatalytic activity is site selectivity of  $\text{Fe}^{3+}$  modification. The following experiments were carried out to determine the reason.

The same modification method was applied to commercial rutile  $\text{TiO}_2$  without specific exposed crystal faces. Therefore, UV irradiation during  $\text{Fe}^{3+}$  modification is thought to induce non-site-selective modification on the particles because a redox reaction proceeds in the neighboring sites without being separated. The amounts of evolved  $\text{CO}_2$  evolution as a result of decomposition of acetaldehyde over site-selective and non-site-selective  $\text{Fe}^{3+}$ -modified commercial rutile  $\text{TiO}_2$  were  $495 \times 10^{-6}$  and  $500 \times 10^{-6}$ , respectively under visible light irradiation for 24 h. These two samples were prepared by different modification methods, but the same net amounts of  $\text{Fe}^{3+}$  compound were loaded on these rutile samples by adjusting the initial amount of  $\text{Fe}^{3+}$ . The photocatalytic activities of these samples were similar with or without UV irradiation during  $\text{Fe}^{3+}$  modification. This indicates that the UV irradiation induced formation of the same  $\text{Fe}^{3+}$  species for

photocatalytic reaction as that in the case of non-site-selective modification of  $\text{Fe}^{3+}$  on a rutile  $\text{TiO}_2$  nanorod. Therefore, the reason for the high activity of site-selective  $\text{Fe}^{3+}$  modified samples is that UV irradiation during  $\text{Fe}^{3+}$  modification induces loading of site-selective  $\text{Fe}^{3+}$  compounds on rutile  $\text{TiO}_2$  nanorod.

Properties of electron injection in the conduction band of  $\text{TiO}_2$  were observed by DB-PAS [35]. [Figure 8](#) shows PA intensities for a non-site-selective  $\text{Fe}^{3+}$ -modified rutile  $\text{TiO}_2$  nanorod and a site-selective  $\text{Fe}^{3+}$ -modified rutile  $\text{TiO}_2$  nanorod as a function of irradiation time of visible-light in the presence of  $\text{N}_2+\text{EtOH}$ . PA intensity increased with visible light irradiation because  $\text{Ti}^{4+}$  was reduced to  $\text{Ti}^{3+}$  by injected electrons from the photoexcited  $\text{Fe}^{3+}$  compound loaded on the rutile  $\text{TiO}_2$  nanorod. The saturation limit of PA intensity showed no dependence on  $\text{Fe}^{3+}$  modification conditions. This is a reasonable result because the amounts of photoabsorption of these samples were not so different as shown in [Fig. 6](#). This indicates that the plausible factor may be efficiency of reduction on rutile  $\text{TiO}_2$  nanorods modified with  $\text{Fe}^{3+}$  by injected electrons.

DB-PA measurements in the presence of oxygen with EtOH were also carried out to elucidate the behavior of injected electrons in the rutile  $\text{TiO}_2$  nanorod. [Figure 9](#) shows time-course curves of a non-site-selective  $\text{Fe}^{3+}$ -modified rutile  $\text{TiO}_2$  nanorod and a site-selective  $\text{Fe}^{3+}$ -modified rutile  $\text{TiO}_2$  nanorod under visible-light irradiation in the presence of air+EtOH. The steady-state value of PA intensity showed a dependence on the modification method (non-site-selective  $\text{Fe}^{3+}$ -modified rutile  $\text{TiO}_2$  nanorod > site-selective  $\text{Fe}^{3+}$ -modified rutile  $\text{TiO}_2$  nanorod). This suggests that the efficiency of reduction on the surface of a site-selective  $\text{Fe}^{3+}$ -modified rutile  $\text{TiO}_2$  nanorod is higher than that on a non-site-selective  $\text{Fe}^{3+}$ -modified rutile  $\text{TiO}_2$  nanorod because the consumption of injected electrons in the rutile  $\text{TiO}_2$  nanorod by reduction of oxygen efficiently proceeded on the {110} face without retardation.

#### **4. Morphology-controlled brookite $\text{TiO}_2$ nanorod with exposed crystal faces**

Morphology-controlled brookite  $\text{TiO}_2$  nanorods with {210} and {212} exposed crystal faces were prepared by hydrothermal synthesis [19, 37-42]. The procedure for preparation of morphology-controlled brookite  $\text{TiO}_2$  with exposed crystal faces is as follows. Amorphous titanium hydroxide particles were dispersed in 30% hydrogen peroxide containing ammonia and glycolic acid. After stirring the solution at **ca.** 60 °C for several hours, an orange gelled compound was obtained. The gelled compound was dispersed in deionized water with pH being adjusted to 10 by the addition of ammonia. The solution in a Teflon bottle sealed with a stainless jacket was heated at 200 °C for 48 h in an oven. After hydrothermal treatment, the residue was washed with deionized water and dried under reduced pressure at 60 °C for 12 h.



For controlling the aspect ratio (AR) of brookite of a TiO<sub>2</sub> nanorod, the preparation procedure was modified as follows. Amorphous titanium hydroxide particles were dispersed in 30% hydrogen peroxide containing ammonia and glycolic acid, and a yellow peroxy titanate (PTA) solution was obtained. An aqueous solution containing an appropriate amount of PVA (5, 25, or 50 mg) was added to the PTA solution and the solution was stirred at room temperature for 6 h. After the treatment, an orange gelled compound was obtained. The gelled compound was dispersed in deionized water with pH being adjusted to 10. The solution in a Teflon bottle sealed with a stainless jacket was heated at 200 °C for 48 h in an oven. After hydrothermal treatment, the residue in the Teflon bottle was washed with milli-Q water until ionic conductivity of the supernatant was < 10 S·cm<sup>-1</sup>. The particles were dried under reduced pressure at 60 °C for 12 h.

Figure 11 shows XRD patterns of prepared TiO<sub>2</sub> nanorod particles, which are assigned to a pure brookite phase. Surface areas of the brookite TiO<sub>2</sub> nanorods prepared with 5, 25 and 50 mg of PVA were 24.2, 25.8, and 27.7 m<sup>2</sup>·g, respectively. Figure 12 shows TEM image of brookite TiO<sub>2</sub> without a polymer. A brookite TiO<sub>2</sub> nanorod with a length of 100 nm, width of 25 nm and AR of 2.7 was obtained. The relative surface area of the prepared brookite TiO<sub>2</sub> nanorod was 47 m<sup>2</sup>·g<sup>-1</sup>. Exposed crystal faces were analyzed by TEM and SAED analysis and were assigned to large {212} and small {210} exposed crystal faces (Fig. 11). The {210} and {212} exposed crystal faces on the brookite TiO<sub>2</sub> nanorod were assigned to reduction and oxidation sites using previously reported technique [15-17]. Therefore, Fe<sup>3+</sup> are expected to mainly adsorb on {212} faces under UV irradiation because Fe<sup>3+</sup> on {210} faces desorb due to reduction of Fe<sup>3+</sup> to Fe<sup>2+</sup> (Fig.5). Fe<sup>2+</sup> were recovered to Fe<sup>3+</sup> as a result of reoxidation by oxygen and/or positive holes on {212} faces.

TEM images of AR-controlled brookite TiO<sub>2</sub> by addition of the PVA polymer are shown in Fig.12. The results indicate that addition of 50 mg PVA was sufficient to prepare brookite TiO<sub>2</sub> particles with the smallest AR (Fig. 12). TEM images of samples prepared with and without PVA are shown in Fig. 13.

Photocatalytic activities for photocatalytic decomposition of toluene over a brookite TiO<sub>2</sub> nanorod were evaluated. 100 mg powder was spread on a glass dish, which was placed in a Tedlar bag. Five hundred parts per million of gaseous acetaldehyde or one hundred parts per million of gaseous toluene was injected into the Tedlar bag. The gaseous composition in the Tedlar bag was 79% N<sub>2</sub>, 21% O<sub>2</sub>, < 0.1×10<sup>-6</sup> CO<sub>2</sub> and 100×10<sup>-6</sup> or 500×10<sup>-6</sup> toluene, and relative humidity was ca. 30%. A light-emitting diode with a center wavelength of ca. 365 nm (0.1 mW·cm<sup>-2</sup>) was used as the light source. The concentrations of acetaldehyde and carbon dioxide (CO<sub>2</sub>) were analyzed by gas chromatography.

The photocatalytic activities of the prepared samples for decomposition of toluene were evaluated. [Figure 14](#) shows CO<sub>2</sub> evolution as a result of toluene decomposition over several kinds of brookite TiO<sub>2</sub> under UV LED irradiation for 8 h. The AR of a brookite TiO<sub>2</sub> nanorod with specific exposed crystal faces was rather sensitive to photocatalytic activity for toluene decomposition. Toluene decomposition on a photoirradiated brookite TiO<sub>2</sub> nanorod with a larger AR showed higher photocatalytic activity than that on a brookite TiO<sub>2</sub> nanorod with a smaller AR. This result suggested that photocatalytic activity for toluene decomposition increased with an increase in the AR of the brookite TiO<sub>2</sub> nanorod. Under optimized conditions, reduction sites on the surface of the brookite TiO<sub>2</sub> nanorod should be predominantly exposed as shown in [Fig. 14](#). These results indicated that reduction of oxygen on the surfaces of the reduction sites of a brookite TiO<sub>2</sub> nanorod might be the rate-determining step for toluene oxidation over a brookite TiO<sub>2</sub> nanorod under UV light.

### 5. Visible light-responsive brookite TiO<sub>2</sub> nanorod modified with Fe<sup>3+</sup> compounds

For non-site-selective Fe<sup>3+</sup> compound modification of a brookite TiO<sub>2</sub> nanorod, an aqueous suspension containing shape-controlled brookite TiO<sub>2</sub> nanorods and an aqueous solution of iron(III) nitrate (Fe(NO<sub>3</sub>)<sub>3</sub>) was stirred for 6 h under an aerated condition. The supernatant and residue were separated by filtration, and the residue was washed with deionized water and dried under reduced pressure.

For site-selective Fe<sup>3+</sup> compound modification of a brookite TiO<sub>2</sub> nanorod, an aqueous suspension containing each brookite TiO<sub>2</sub> and an aqueous solution of Fe(NO<sub>3</sub>)<sub>3</sub> with ethanol was stirred for 6 h under an aerated condition. The stirring was carried out under UV irradiation with a 500-W super-high-pressure mercury lamp (1.0 mW·cm<sup>-2</sup>). The supernatant and residue were separated by filtration immediately after stirring for 6 h. The residue was washed with deionized water and dried under reduced pressure.

The color of the brookite TiO<sub>2</sub> nanorod changed from white to pale yellow. [Figure 15](#) shows UV-Vis spectra of bare and Fe<sup>3+</sup>-modified brookite TiO<sub>2</sub>. An increase in photoabsorption was observed in the wavelength region between 400 and 500 nm of DR spectra. Photoabsorption increased with an increase in the net amount of Fe<sup>3+</sup> compounds loaded on the brookite TiO<sub>2</sub> nanorod.

Photocatalytic activities for decomposition of acetaldehyde over the samples were analyzed. 100 mg powder was spread on a glass dish, which was placed in a 125 cm<sup>3</sup> Tedlar bag. **Five hundred parts per million** of gaseous acetaldehyde was injected into the Tedlar bag. The gaseous composition in the Tedlar bag was 79% N<sub>2</sub>, 21% O<sub>2</sub>, < 0.1×10<sup>-6</sup> CO<sub>2</sub> and 500×10<sup>-6</sup> acetaldehyde,

and relative humidity was **ca.** 30%. A light-emitting diode (LED, Lumileds, Luxeon LXHL-NRR8) that emitted light at a wavelength of 455 nm ( $1.0 \text{ mW}\cdot\text{cm}^{-2}$ ) was used. The concentrations of acetaldehyde and carbon dioxide ( $\text{CO}_2$ ) were estimated by gas chromatography.

Figure 16 shows the dependence of the site-selective  $\text{Fe}^{3+}$  compound-modified brookite  $\text{TiO}_2$  on photocatalytic activity ( $\text{CO}_2$  evolution as a result of acetaldehyde degradation after 24 h of photoirradiation). Photocatalytic activity of the  $\text{Fe}^{3+}$ -modified brookite  $\text{TiO}_2$  nanorod was much higher than that of the  $\text{Fe}^{3+}$ -modified commercial spherical brookite  $\text{TiO}_2$ . Under visible light irradiation, no photocatalytic activity of the bare brookite  $\text{TiO}_2$  nanorod or bare commercial brookite  $\text{TiO}_2$  nanoparticles for oxidation of acetaldehyde was observed. This indicates that  $\text{Fe}^{3+}$  on the brookite  $\text{TiO}_2$  nanorod induced photocatalytic reaction under visible-light irradiation [26]. The amount of evolved  $\text{CO}_2$  over nitrogen-doped  $\text{TiO}_2$  (N- $\text{TiO}_2$ ; Sumitomo Chemical Co.) was about  $180 \times 10^{-6}$  under the same experimental conditions. The  $\text{Fe}^{3+}$ -modified brookite  $\text{TiO}_2$  nanorod showed much higher photocatalytic activity than that of N- $\text{TiO}_2$ .

Photocatalytic activity increased with an increase in the amount of  $\text{Fe}^{3+}$  modification because of the increase in visible light photoabsorption. In addition, an excess amount of  $\text{Fe}^{3+}$  modification decreased photocatalytic activity presumably due to a decrease in reduction sites by coverage of the  $\text{TiO}_2$  surface. Therefore, an increase in photocatalytic activity of the site-selective  $\text{Fe}^{3+}$ -modified brookite  $\text{TiO}_2$  nanorod might be attributable to the removal of an excess amount of  $\text{Fe}^{3+}$  compounds. In addition, a site-selective  $\text{Fe}^{3+}$  modified brookite  $\text{TiO}_2$  nanorod with a larger AR showed higher photocatalytic activity for acetaldehyde degradation than that of a brookite  $\text{TiO}_2$  nanorod site-selectively modified with  $\text{Fe}^{3+}$  compounds having a smaller AR. These results suggested that the rate-determining step of acetaldehyde oxidation under visible light might be oxygen reduction proceeding on the reduction site of the brookite  $\text{TiO}_2$  nanorod. Therefore, a site-selective  $\text{Fe}^{3+}$  modified brookite  $\text{TiO}_2$  nanorod with a larger AR having a large reduction area showed the highest activity for acetaldehyde oxidation under visible light.

The same modification method was applied to commercial brookite  $\text{TiO}_2$  that has a spherical shape without specific exposed crystal faces. Figure 16 shows the amount of  $\text{CO}_2$  evolution over site-selective  $\text{Fe}^{3+}$ -modified commercial brookite  $\text{TiO}_2$  nanoparticles under visible-light irradiation. The photocatalytic activity of  $\text{Fe}^{3+}$ -modified commercial brookite  $\text{TiO}_2$  is quite low compared to that of the site-selective  $\text{Fe}^{3+}$ -modified brookite  $\text{TiO}_2$  nanorod because UV irradiation during  $\text{Fe}^{3+}$  modification does not induce site-selective modification on the commercial brookite  $\text{TiO}_2$  nanoparticles due to the redox reaction proceeding in the neighboring sites without being separated.

## 6. Conclusion

It is demonstrated that the morphology of rutile and brookite TiO<sub>2</sub> particles can be controlled by means of a hydrothermal process with morphology-controlled reagents. The addition of PVP and PVA to the hydrothermal preparation process for a brookite TiO<sub>2</sub> nanorod reduces the AR of the brookite TiO<sub>2</sub> nanorod (AR ~ 1.6-5.2). The exposed crystal surfaces of rutile and brookite TiO<sub>2</sub> nanorods show different activities: oxidation and reduction. The photocatalytic activities of rutile and brookite TiO<sub>2</sub> nanorods are higher than that of anatase or brookite TiO<sub>2</sub> fine particles that are commercially available in Japan. It is found that the photocatalytic activity depends not on the relative surface area but on the surface structure of TiO<sub>2</sub> nanorods, suggesting that prevention of electron-hole pair recombination plays an important role during the photodegradation of organic compounds.

Fe<sup>3+</sup>-modification on shape-controlled rutile and brookite TiO<sub>2</sub> nanorods results in high photocatalytic activity under visible-light irradiation because Fe<sup>3+</sup> are site-selectively modified on {111} and {212} exposed crystal faces and redox reactions are spatially separated. DB-PA analyses indicate that photocatalytic activity is determined by not efficiency of electron injection but efficiency of reduction by injected electrons. The efficiency of reduction is influenced by site-selectivity of Fe<sup>3+</sup>-modification on {111} faces because Fe<sup>3+</sup> on {110} faces retard an efficient reduction on the bare TiO<sub>2</sub> surface.

## Acknowledgements

**This work was financially supported by the Advanced Catalytic Transformation Program for Carbon Utilization (ACT-C), Japan Science and Technology Agency (JST).**

## References

- [1] Yu J, Low J, Xiao W, Zhou P, Jaroniec M. Enhanced Photocatalytic CO<sub>2</sub>-Reduction Activity of Anatase TiO<sub>2</sub> by Coexposed {001} and {101} Facets. *J. Am. Chem. Soc.* 2014 :136 :8839.
- [2] Huang Z, Sun , Lv K, Zhang Z, Li M, Li B. Effect of contact interface between TiO<sub>2</sub> and g-C<sub>3</sub>N<sub>4</sub> on the photoreactivity of g-C<sub>3</sub>N<sub>4</sub>/TiO<sub>2</sub> photocatalyst: (0 0 1) vs (1 0 1) facets of TiO<sub>2</sub>. *Appl. Catal. B : Environmental.* 2015 :164 :420.
- [3] Zhou P, Wu J, Yu W, Zhao G, Fang G, Cao S. Vectorial doping-promoting charge transfer in anatase TiO<sub>2</sub> {0 0 1} surface. *Appl. Sur. Sci.* 2014 :319 :167.

- [4] Wang C, Hu Q, Huang J, Zhu C, Deng Z, Shi H, Wu L, Liu Z, Cao Y. Enhanced hydrogen production by water splitting using Cu-doped TiO<sub>2</sub> film with preferred (0 0 1) orientation. *Appl. Sur. Sci.* 2014 :292 :161.
- [5] Ren C, Wang G, Chen Y, Chen Y. Degradation of benzene on Zr-doped TiO<sub>2</sub> photocatalysts with a bimodal pore size distribution. *Rare Metals.* 2014 :33 :714.
- [6] Lv K, Cheng B, Yu J, and Liu G. Fluorine ions-mediated morphology control of anatase TiO<sub>2</sub> with enhanced photocatalytic activity. *Phys. Chem. Chem. Phys.* 2012 :14 :5349.
- [7] Hoffmann M R, Martin S T, Choi W, Bahnemann D W. Environmental applications of semiconductor photocatalysis. *Chem Rev.* 1995 : 95:69.
- [8] Choi W. Pure and modified TiO<sub>2</sub> photocatalysts and their environmental applications. *Catal Surv Asia.* 2006 : 10 :16.
- [9] Chen X, Mao S S. Titanium dioxide nanomaterials: Synthesis, properties, modifications, and applications. *Chem Rev.* 2007 : 107:2891
- [10] Hosono E, Fujihara S, Kakiuchi K, Imai H. Growth of submicrometer-scale rectangular parallelepiped rutile TiO<sub>2</sub> films in aqueous TiCl<sub>3</sub> solutions under hydrothermal conditions. *J Am Chem Soc.* 2004 : 126:7790.
- [11] Neale N R, Frank A J. Size and shape control of nanocrystallites in mesoporous TiO<sub>2</sub> films. *J Mater Chem.* 2007 17:3216.
- [12] Huang X, Pan C. Large-scale synthesis of single-crystalline rutile TiO<sub>2</sub> nanorods via a one-step solution route. *J Cryst Growth.* 2007 : 306:117.
- [13] Testino A, Bellobono I R, Buscaglia V, Canevali C, D'Arienzo M, Polizzi S, Scotti R, Morazzoni F. Optimizing the photocatalytic properties of hydrothermal TiO<sub>2</sub> by the control of phase composition and particle morphology. A systematic approach. *J Am Chem Soc.* 2007 : 129:3564.
- [14] Ohno T, Sarukawa K, Matsumura M. Crystal faces of rutile and anatase TiO<sub>2</sub> particles and their roles in photocatalytic reactions. *New J Chem.* 2002 : 26:1167.
- [15] Bae E, Murakami N, Ohno T. Exposed crystal surface-controlled TiO<sub>2</sub> nanorods having rutile phase from TiCl<sub>3</sub> under hydrothermal conditions. *J Mol Catal A: Chem.* 2009 : 300:72.
- [16] Bae E, Ohno T. Exposed crystal surface-controlled rutile TiO<sub>2</sub> nanorods prepared by hydrothermal treatment in the presence of poly(vinyl pyrrolidone). *Appl Catal B: Environ.* 2009 : 91: 634.
- [17] Bae E, Murakami N, Nakamura M, Ohno T. Effect of chemical etching by sulfuric acid or H<sub>2</sub>O<sub>2</sub>-NH<sub>3</sub> mixed solution on the photocatalytic activity of rutile TiO<sub>2</sub> nanorods. *Appl Catal A: Gen.* 2010 : 380:48

- [18] Murakami N, Kurihara Y, Tsubota T, Ohno T. Shape-controlled anatase titanium(IV) oxide particles prepared by hydrothermal treatment of peroxy titanate acid in the presence of polyvinyl alcohol. *J Phys Chem C*. 2009 : 113:3062.
- [19] Ohno T, Higo T, Saito H, Yuan S, Jin Z, Yang Y, Tsubota T. Dependence of photocatalytic activity on aspect ratio of a brookite TiO<sub>2</sub> nanorod and drastic improvement in visible light responsibility of a brookite TiO<sub>2</sub> nanorod by site-selective modification of Fe<sup>3+</sup> on exposed faces. *J Mol Catal A: Chem*. 2015 : 396:261.
- [20] Sato, S. Photocatalytic activity of NO<sub>x</sub>-doped TiO<sub>2</sub> in the visible-light region. *Chem Phys Lett*. 1986 ; 123:126.
- [21] Asahi R, Morikawa, T, Ohwaki T, Aoki K, Taga Y. Visible-light photocatalysis in nitrogen-doped titanium oxides. *Science*. 2001 : 293:269.
- [22] Umebayashi T, Yamaki T, Itoh H, Asai K. Band gap narrowing of titanium dioxide by sulfur doping. *Appl Phys Lett*. 2002 : 81:454.
- [23] Ohno T, Akiyoshi M, Umebayashi T, Asai K, Mitsui T, Matsumura M. Preparation of S-doped TiO<sub>2</sub> photocatalysts and their photocatalytic activities under visible light. *Appl Catal A: Gen*. 2004 : 265:115.
- [24] Ohno T, Tsubota T, Nishijima K, Miyamoto Z. Degradation of methylene blue on carbonate species-doped TiO<sub>2</sub> photocatalysts under visible light. *Chem Lett*. 2004 : 33:750.
- [25] Irie H, Watanabe Y, Hashimoto K. Carbon-doped anatase TiO<sub>2</sub> powders as a visible-light sensitive photocatalyst. *Chem Lett*. 2003 : 32:772.
- [26] Serpone N, Lawless D. Spectroscopic, photoconductivity, and photocatalytic studies of TiO<sub>2</sub> colloids - naked and with the lattice doped with Cr<sup>3+</sup>, Fe<sup>3+</sup>, and V<sup>5+</sup> cations. *Langmuir*. 1994 : 10:643.
- [27] Ikeda S, Sugiyama N, Pal B, Marci G, Palmisano L, Noguchi H, Uosaki K, Ohtani B. Photocatalytic activity of transition-metal-loaded titanium(IV) oxide powders suspended in aqueous solutions: Correlation with electron-hole recombination kinetics. *Phys Chem Chem Phys*. 2001 : 3:267.
- [28] Kisch H, Zang L, Lange C, Maier W F, Antonius C, Meissner D. Modified, amorphous titania - a hybrid semiconductor for detoxification and current generation by visible light. *Angew Chem Int Ed*. 1998 : 37: 3034.
- [29] Zang L, Lange C, Abraham I, Storck S, Maier W F, Kisch H. *J. Phys. Chem. B*. 1998 : 102:10765.

- [30] Zang L, Lange C, Abraham I, Storck S, Maier W F, Kisch H. Amorphous microporous titania modified with platinum(IV) chloride - A new type of hybrid photocatalyst for visible light detoxification. *J Phys Chem B*. 1998 : 102:10765.
- [31] Macyk W, Kisch H. Photosensitization of crystalline and amorphous titanium dioxide by platinum(IV) chloride surface complexes. *Chem Eur J*. 2001 : 7:1862.
- [32] Murakami N, Chiyoya T, Tsubota T, Ohno T. Switching redox site of photocatalytic reaction on titanium(IV) oxide particles modified with transition-metal ion controlled by irradiation wavelength. *Appl Catal A: Gen*. 2008 : 348:148.
- [33] Murakami N, Ono A, Nakamura M, Tsubota T, Ohno T. Development of a visible-light-responsive rutile rod by site-selective modification of iron(III) ion on {111} exposed crystal faces. *Appl Catal A: Gen*. 2010 : 97:115.
- [34] Oliver P M, Watson G W, Kelsey E T, Parker. S C. Atomistic simulation of the surface structure of the TiO<sub>2</sub> polymorphs rutile and anatase. *J Mater Chem*. 1997 : 7:563.
- [35] Murakami N, Mahaney O O P, Abe R, Torimoto T, Ohtani B. Double-beam photoacoustic spectroscopic studies on transient absorption of titanium(IV) oxide photocatalyst powders. *J Phys Chem C*. 2007 : 111:11927.
- [36] Ohno T, Haga D, Fujihara K, Kaizaki K, Matsumura M. Unique effects of iron(III) ions on photocatalytic and photoelectrochemical properties of titanium dioxide. *J Phys Chem B*. 1997 : 101:6415.
- [37] Kandiel T A, Feldhoff A, Robben L, Dillert R, Bahnemann D W. Tailored titanium dioxide nanomaterials: anatase nanoparticles and brookite nanorods as highly active photocatalysts. *Chem Mater*. 2010 : 22:2050.
- [38] Kobayashi M, Tomita K, Petrykin V, Yin S, Sato T, Yoshimura M, Kakihana M. Hydrothermal synthesis of nanosized titania photocatalysts using novel water-soluble titanium complexes. *Solid State Phenomena*. 2007 : 124-126 :723.
- [39] Zhang H, Banfield J F. Understanding polymorphic phase transformation behavior during growth of nanocrystalline aggregates: insights from TiO<sub>2</sub>. *J Phys Chem B*. 2000 : 104 :3481.
- [40] Kobayashi M, Petrykin V, Kakihana M, Tomita K. Hydrothermal synthesis and photocatalytic activity of whisker-like rutile-type titanium dioxide. *J Am Ceram Soc*. 2009: 92(S1): S21.
- [41] Murakami N, Kamai T, Tsubota T, Ohno T. Novel hydrothermal preparation of pure brookite-type titanium(IV) oxide nanocrystal under strong acidic condition. *Catal. Commun*. 2009 : 10 :963.

[42] Ma Z, Zhang Q, Liu J, Yan C, Zhang M, Ohno T. Preparation of luminescent polystyrene microspheres via surface-modified route with rare earth ( $\text{Eu}^{3+}$  and  $\text{Tb}^{3+}$ ) complexes linked to 2, 2'-bipyridine. *Rare Metals*. 2013; 30: 1.



Figs

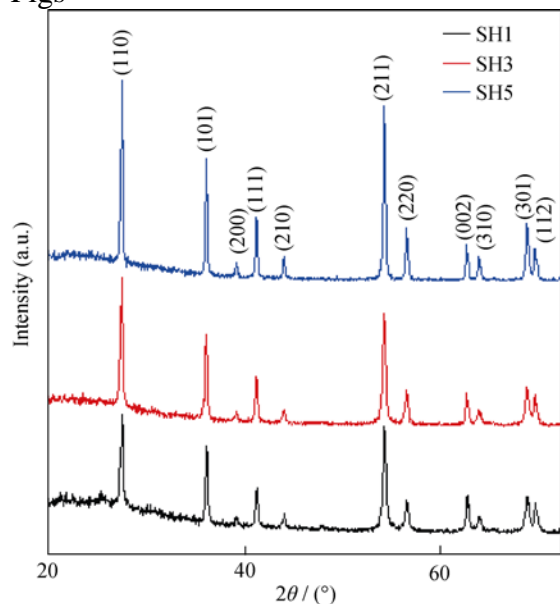


**Fig. 1** XRD patterns of SH1, SH3, and SH5.

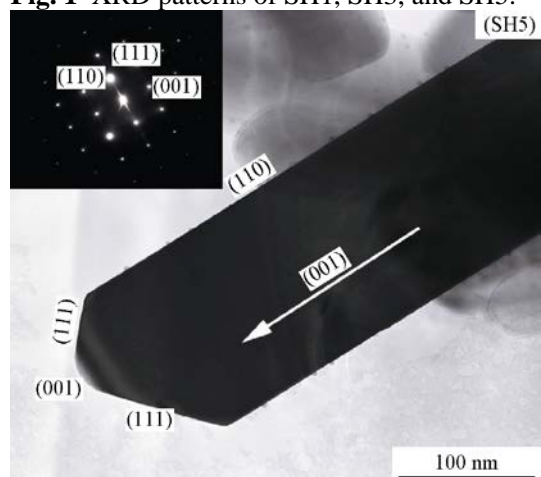


**Fig. 2** TEM image and SAED pattern (insert) of SH5.

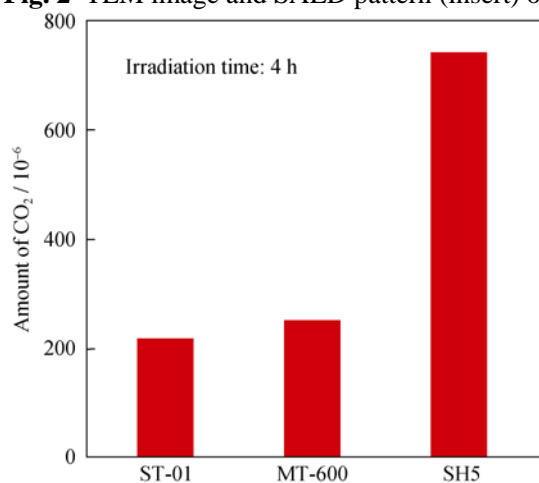


**Fig. 3** Amount of evolved CO<sub>2</sub> as a result of decomposition of acetaldehyde on rutile TiO<sub>2</sub> nanorod. Light intensity: 10 mW·cm<sup>-2</sup>, irradiation time: 4h, acetaldehyde: 500×10<sup>-6</sup>

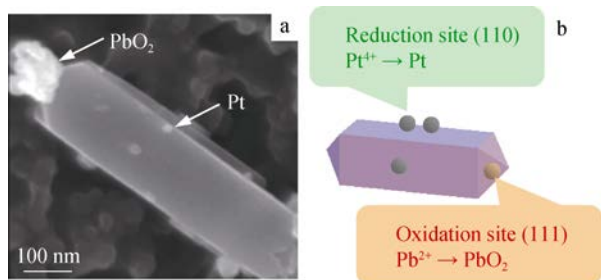


**Fig. 4** SEM image of rutile TiO<sub>2</sub> nanorod on which Pt and PbO<sub>2</sub> particles being deposited for reduction site and oxidation site, respectively **a**; schematic representation of Pt or PbO<sub>2</sub> deposition mechanism and assignment of reaction sites **b**.

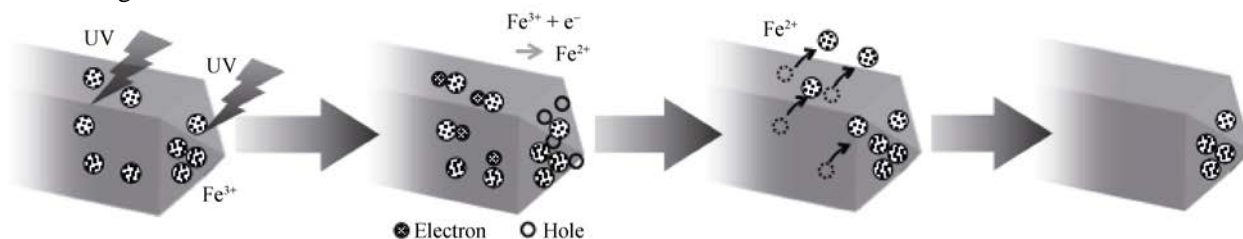


**Fig.5** Site selective modification on shape controlled rutile rod with {110} and {111} exposed crystal faces

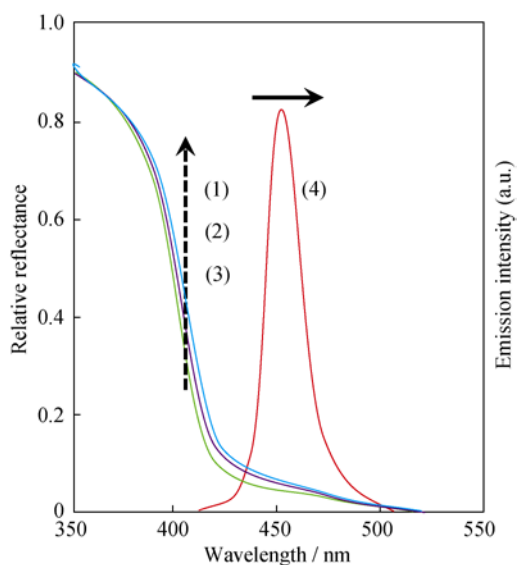


**Fig. 6** UV-Vis spectra of (1) non-site-selective Fe<sup>3+</sup> modified rutile TiO<sub>2</sub> nanorod, (2) site-selective Fe<sup>3+</sup> modified rutile TiO<sub>2</sub> nanorod, (3) rutile TiO<sub>2</sub> nanorod without modification of Fe<sup>3+</sup> compounds and (4) emission spectrum of LED used for photocatalytic evaluation

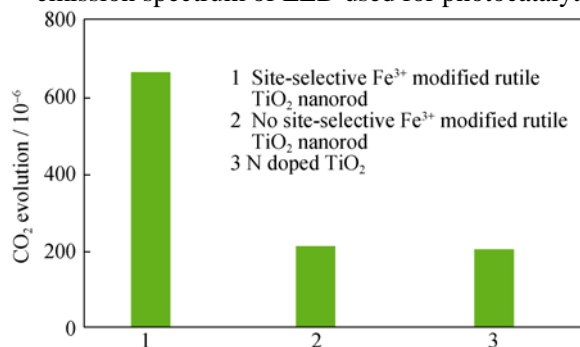


**Fig. 7** Amount of evolved CO<sub>2</sub> as a result of acetaldehyde decomposition over Fe<sup>3+</sup> modified rutile TiO<sub>2</sub> nanorod and N-doped TiO<sub>2</sub> under visible-light irradiation

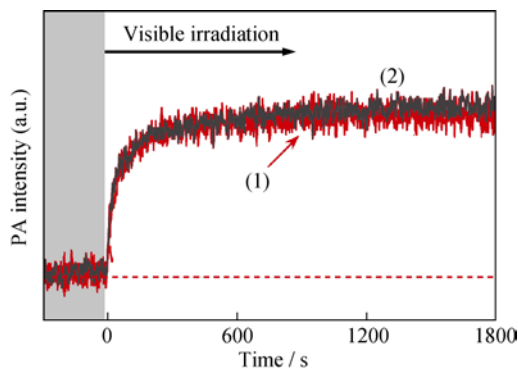


**Fig. 8** Time-course curves of PA signals of (1) no site-selective  $\text{Fe}^{3+}$  modified rutile  $\text{TiO}_2$  nanorod and (2) site-selective  $\text{Fe}^{3+}$  modified rutile  $\text{TiO}_2$  nanorod under visible-light irradiation in presence of  $\text{N}_2+\text{EtOH}$

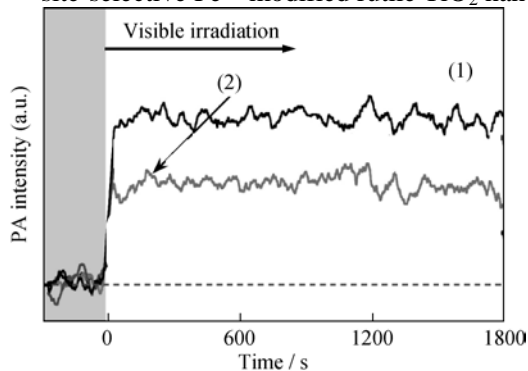


**Fig. 9** Time-course curves of PA signals with 50 points smoothing of (1) no site-selective  $\text{Fe}^{3+}$  modified rutile  $\text{TiO}_2$  nanorod and (2) site-selective  $\text{Fe}^{3+}$  modified rutile  $\text{TiO}_2$  nanorod under visible-light irradiation in presence of air + EtOH

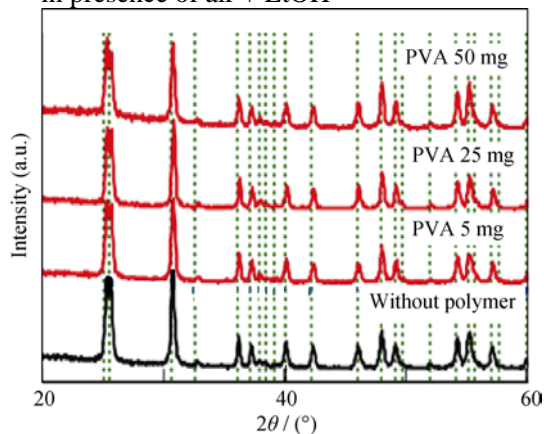


**Fig. 10** XRD patterns of prepared  $\text{TiO}_2$  nanorods.

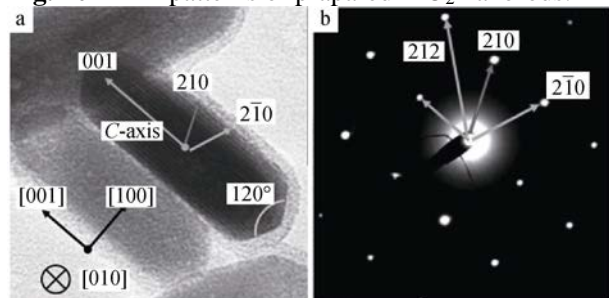


**Fig. 11** TEM image of brookite  $\text{TiO}_2$  nanorod **a** and SAED analysis of prepared brookite  $\text{TiO}_2$  without a polymer **b**

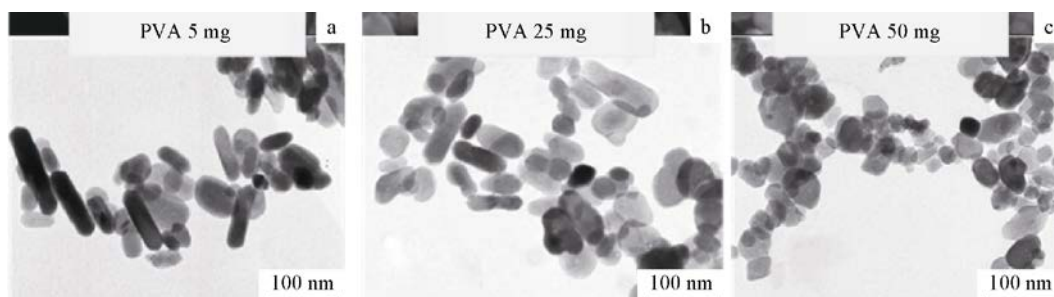


**Fig. 12** Influence of addition of PVA on aspect ratio (AR) of brookite  $\text{TiO}_2$  nanorods: **a** 5 mg, **b** 25 mg, and **c** 50 mg.

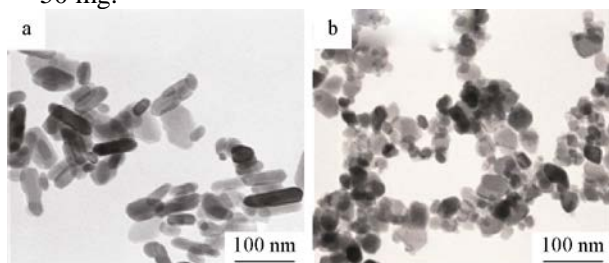


**Fig. 13** TEM images of prepared brookite  $\text{TiO}_2$  nanorod: **a** AR=2.7, without a polymer; **b** AR=1.6, with PVA (50 mg)

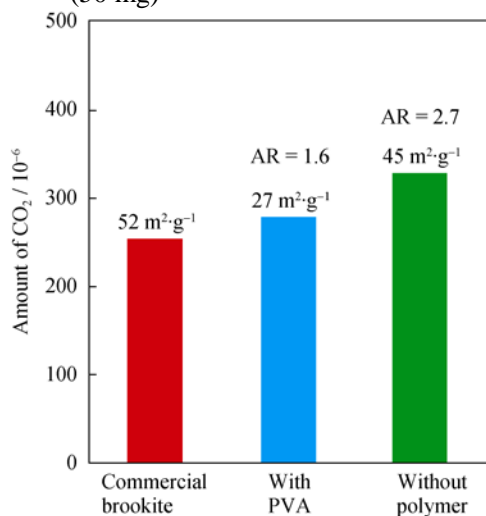


**Fig. 14**  $\text{CO}_2$  evolution as a result of toluene decomposition over three kinds of prepared brookite  $\text{TiO}_2$  under UV LED irradiation for 8 h

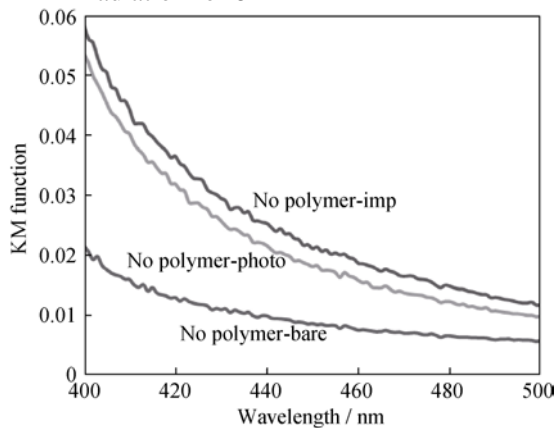


**Fig. 15** UV-Vis spectra of bare and  $\text{Fe}^{3+}$  (0.05 wt%)-modified brookite  $\text{TiO}_2$  without a polymer. Imp meaning non-site-selective  $\text{Fe}^{3+}$  compound modification of brookite  $\text{TiO}_2$  and photo meaning site-selective  $\text{Fe}^{3+}$  compound modification of brookite  $\text{TiO}_2$ .

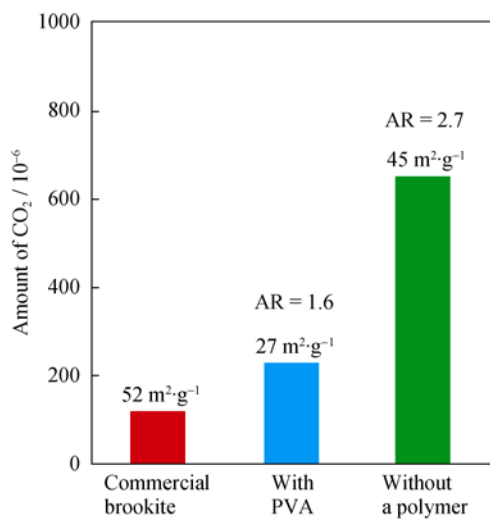


**Fig. 16** CO<sub>2</sub> evolution as a result of acetaldehyde decomposition over several kinds of Fe<sup>3+</sup> (0.05 wt%)-modified brookite TiO<sub>2</sub> under visible light irradiation for 24 h by using an LED at a wavelength of 455 nm